Atmos. Chem. Phys. Discuss., 4, 8171–8199, 2004
www.atmos-chem-phys.org/acpd/4/8171/
SRef-ID: 1680-7375/acpd/2004-4-8171
European Geosciences Union

Atmospheric Chemistry and Physics Discussions

4-D comparison method to study the NO_y partitioning in summer polar stratosphere – Influence of aerosol burden

G. Dufour[1], S. Payan[1], F. Lefèvre[2], M. Eremenko[1], A. Butz[3], P. Jeseck[1], Y. Té[1], K. Pfeilsticker[3], and C. Camy-Peyret[1]

[1]Laboratoire de Physique Moléculaire et Applications, Université P. et M. Curie, Paris, France
[2]Service d'Aéronomie, Institut Pierre-Simon Laplace, Paris, France
[3]Institut für Umweltphysik, University of Heidelberg, Germany

Received: 12 May 2004 – Accepted: 1 September 2004 – Published: 10 December 2004

Correspondence to: G. Dufour (gdufour@acebox.uwaterloo.ca)

Abstract

On 21–22 August 2001, NO, NO_2 and HNO_3 mixing ratio profiles were measured at high latitudes during sunset and sunrise using the Limb Profile Monitor of the Atmosphere (LPMA) and the DOAS experiments under stratospheric balloon. Photochemical simulations using the chemistry module of the Reprobus Chemistry Transport Model (CTM) that are constrained by ozone and total NO_y balloon observations reproduce well the partitioning of NO_x and NO_y when model results are calculated at the exact time and location of the measurement for each tangent altitude. Taking the recently recommended reaction rate coefficients for the NO_y partitioning (JPL-2003) and using realistic aerosol surface area in order to initialise the model leads to an agreement between calculations and measurements better than 10% all over the covered altitude range.

1. Introduction

Stratospheric ozone loss results mainly from catalytic cycles involving reactive nitrogen (NO_x), hydrogen (HO_x) and halogens (ClO_x and BrO_x) species. In the lower stratosphere, the nitrogen radicals (NO_x=NO+NO_2) play an important role by catalytically removing ozone and by moderating indirectly ozone loss through the coupling between the different radical families (Wennberg et al., 1994) and the formation of reservoir molecules. Many studies on nitrogen species, in particular addressing the polar winter stratosphere (Lary et al., 1997; Wetzel et al., 1997), demonstrated that for NO_y the differences between model and measurement values are often larger than several ten percents. In particular the NO_2 volume mixing ratio, the NO_2/HNO_3 ratio and the NO_x/NO_y (NO_y=NO_x+NO_3+HNO_3+2×N_2O_5+HNO_2+HNO_4+$ClONO_2$+$BrONO_2$) ratio are found to largely disagree in the lower stratosphere below 30 km. In order to improve the photochemical models, a better understanding of the partitioning of NO_x and NO_y is thus needed. The NO/NO_2 ratio is controlled by fast photochemistry which

ACPD
4, 8171–8199, 2004

inter-converts NO and NO_2, mainly through Reactions (R1) and (R2):

$$NO_2 + h\nu \rightarrow NO + O \quad \text{(R1)}$$

$$NO + O_3 \rightarrow NO_2 + O_2 \quad \text{(R2)}$$

The partitioning between NO_2 and HNO_3, and consequently between NO_x and NO_y, is dominated by slower reactions. In the lower stratosphere, the dominant sink of NO_x is a two-step process involving the formation of N_2O_5 during the night, followed by the heterogeneous hydrolysis of N_2O_5 on sulphate aerosols, which converts N_2O_5 to the more stable species HNO_3. In summer at high latitudes, the extended daylight duration is implying efficient photolysis which inhibits the formation of the precursor molecule NO_3 and thus of N_2O_5. In effect, these conditions provide an opportunity to test our understanding of the NO_y partitioning when gas-phase chemistry dominates the exchange between NO_x and HNO_3. Reactions (R3–R5) are the 3 main reactions that govern the NO_2/HNO_3 ratio:

$$HNO_3 + h\nu \rightarrow NO_2 + OH \quad \text{(R3)}$$

$$HNO_3 + OH \rightarrow NO_3 + H_2O \quad \text{(R4)}$$

$$NO_2 + OH + M \rightarrow HNO_3 + M \quad \text{(R5)}$$

Several field studies performed during the 1997 Photochemistry of Ozone Loss in the Arctic Region In Summer (POLARIS) mission investigated the partitioning of NO_y species (Osterman et al., 1999; Gao et al., 1999; Perkins et al., 2001). These studies showed that a significant disagreement between observed and modelled NO_y is observed when using the reaction rates recommended by DeMore et al. (1997). In particular, Osterman et al. (1999) recommended a reduction in the rate coefficient of Reaction (R5) by about 35% to achieve a reasonable agreement (better than 10% for altitudes higher than 15 km and than 30% at lower altitudes) between the modelled and the measured NO_x/NO_y ratio within lower stratosphere. In fact laboratory studies then

undertaken by Brown et al. (1999a, b) showed that k_4 is 20–30% slower than the value recommended by DeMore et al. (1997), whereas k_5 is up to 50% faster. Using this updated rate coefficients Gao et al. (1999) found a significant improvement between modelled and observed NO_x/NO_y ratios for the analysed ER-2 flight.

In the present study, the partitioning of NO_y species is studied using balloon-borne LPMA measurements (Camy-Peyret, 1995) which were performed at high latitude summer and the most recently recommended reaction rates for atmospheric studies (Sander et al., 2003). A robust inter-comparison and initialisation scheme is used to inter-compare observed and simulated profiles of NO, NO_2 and HNO_3 for sunrise and sunset. Here we focus on the ability of the photochemical model to reproduce the observed NO/NO_2 and NO_x/NO_y ratios, taking into account different methods of initialisation of chemical species and stratospheric aerosol load.

2. LPMA observations

The balloon flight reported here took place from Kiruna (Sweden) on 21–22 August 2001. The measurements were performed during three flight phases: balloon ascent from 15:55 UT to 18:42 UT, sunset from 18:43 UT to 20:05 UT and sunrise from 1:11 UT to 2:29 UT. Infrared spectra have been recorded by the LPMA instrument, which is a remote sensing infrared Fourier transform interferometer operating in solar occultation (Camy-Peyret, 1995). The high spectral resolution and sensitivity of the LPMA instrument permits to retrieve vertical profiles of species with stratospheric mixing ratios of the order of a few tenths of ppbv, such as $ClONO_2$. On the same gondola, a UV-visible DOAS (Differential Optical Absorption Spectroscopy) instrument (Ferlemann et al., 2000) analysed the same sun light for O_3 and NO_2 profiles. The ozone profile was also used in this study. Both instruments LPMA and DOAS use the same suntracker to lock onto the sun. Thus, their line of sight (LOS) is identical and the retrieved vertical profiles are directly comparable. The consistency of O_3 and NO_2 retrieved vertical

profiles has been studied in detail (Butz et al., in preparation, 2004 [1]). The LPMA instrument tracked the sun between 10 km up to the float altitude during balloon ascent and until loss of Sun, with a lowest tangent altitude of 12 km, during sunset. Spectra were recorded at sunrise from a tangent altitude of 15 km up to the float altitude of 39 km. Profiles at sunset were retrieved down to 12 km. Tables 1 and 2 summarize the time (UT), the location and the altitude of the tangent points considered in the present study at sunset and sunrise, respectively.

The spectral retrieval of the target species relies on a multifit algorithm that uses an efficient minimization algorithm based on the Levenberg-Marquardt algorithm (Press et al., 1992). It allows the simultaneous detection and retrieval of vertical profiles of CH_4, N_2O, NO, NO_2, HCl, $ClONO_2$ and O_3 in 7 micro-windows. HNO_3 profiles are retrieved using the same algorithm but on a larger spectral window (25 cm^{-1}). All the molecular parameters are extracted from the HITRAN2000 database (Rothmann et al., 2000), except for $ClONO_2$, for which we use the absorption cross-sections measured by Wagner and Birk (2003). The error bars of retrieved NO, NO_2, HNO_3 and $ClONO_2$ volume mixing ratio correspond to 2σ fitting error: they do not include, however, the uncertainties on spectroscopic parameters. These are later added to fitting errors in order to estimate the systematic errors: the total error bars are estimated to 10% for NO and NO_2, to 15% for HNO_3 and to 20% for $ClONO_2$. For tangent heights below 19 km, the spectral micro-window used for the retrieval of ozone is saturated and thus it is difficult to fit correctly the spectrum base line. As a result, the O_3 mixing ratio retrieved from LPMA is underestimated. Consequently, below 19 km, we have used the ozone vertical profiles (for sunset and sunrise) retrieved from the DOAS UV-visible measurements (Butz et al., in preparation, 2004[1]).

[1] Butz, A., Boesch, H., Camy-Peyret, C., et al.: Intercomparison of stratospheric O3 and NO2 profiles by balloon-borne Uv, vis and near-IR solar occultation spectroscopy, 2nd SCIAMACHY ACP Special issue, Atmos. Chem. Phys. Discuss., in preparation, 2004.

3. Comparison method between measurements and model results

The photochemical model used here is a one-dimensional version of the Reprobus chemical-transport model (CTM)(Lefèvre et al., 1994, 1998). The model provides a comprehensive description of the stratospheric chemistry by inclusion of 147 photolytic, gas-phase, and heterogeneous reactions. Most of the used absorption cross-sections, gas-phase reactions, and heterogeneous reaction probabilities are those recommended by the latest JPL compilation (Sander et al., 2003). The aerosol surface area used in the model is inferred from the SAGE-II satellite observations (Thomason et al., 1997). The model extends from the ground up to 0.1 hPa (about 65 km), on 42 vertical levels. We used a short chemical time step of 15 s in order to describe accurately the rapid variations of NO_x species at sunrise and sunset.

Along the line of sight strong spatial variations of the radical species must be taken into account in the retrieval of vertical profiles. The NO volume mixing ratio (vmr) decreases rapidly during sunset and increases rapidly during sunrise. For example, the NO vmr varies by about 20% between 89° and 91° solar zenith angle (SZA). In this case the assumption of a uniform mixing ratio along the line of sight would lead to significant errors. We use the Reprobus 1-D model to calculate the altitude-dependent diurnal variation of NO relative to a SZA reference value of 90°. Derived correcting factors are then used in the retrieval algorithm to correct the NO vmr on each side of the tangent point along the line of sight. The corrected NO profile is compared to the uncorrected one on Fig. 1. The maximum percentage difference reaches more than 85% around 20 km.

For NO_2, the differences between the daytime and night-time concentrations are smaller. Payan et al. (1999) showed that the NO_2 mixing ratio differences between photochemically corrected and uncorrected profiles are less than 6% at any altitude, primarily since the photolysis frequency of NO_2 (J_{NO2}) does not change much in the sunlit part of the stratosphere during sunset/sunrise (Bösch et al., 2001). From a similar measurement technique in absorption (JPL MkIV spectrometer), Sen et al. (1998)

ACPD
4, 8171–8199, 2004

deduced that photochemical corrections of NO_2 profiles are not a significant source of uncertainty. Thus, we did not account for possible variations of the NO_2 abundance along the line of sight.

During the LPMA and DOAS occultation measurements, the location of the tangent point varies by several degrees in latitude and longitude. Vertical profiles of stratospheric species may thus show substantial variations within the area sampled by the instruments. This is illustrated by the output of a three-dimensional simulation of the Reprobus chemical-transport model on 21 August 2001. Figure 2 plots the ozone and NO_2 vertical profiles computed near the two extreme locations of the sunset measurements, for the same solar zenith angle. A large spatial variability is observed, with differences of 1.4 ppmv around the maximum of ozone and 0.7 ppbv for NO_2 (Fig. 2). In order not to introduce additional errors, it is very important to compare measurements and model results at the same time, altitude, longitude and latitude: one must perform a 4-D comparison.

3.0.1. Results and discussion

In this study, the Reprobus 1-D model is initialised shortly before the LPMA measurements at 16:00 UT on 21 August 2001 (sunset) and at 1:00 UT on 22 August 2002 (sunrise). In a first analysis, all species are initialised from the result of a three-dimensional simulation of the Reprobus CTM. The 3-D simulation is initialised on 15 October 2000 and is driven by 6-hourly ECMWF analysis until June 2001. The comparisons between the measured and simulated profiles of NO, NO_2 and HNO_3 retrieved are summarized on Fig. 3. Calculated volume mixing ratio of NO, NO_2 and HNO_3 are underestimated by the Reprobus 1-D model. The disagreement for HNO_3 is explained by the underestimation of the total amount of NO_y in the model. The partitioning between NO_x and NO_y and between NO and NO_2 are shown on Fig. 4. For the NO_x/NO_y ratio (Fig. 4a), the model is simulating well the ratio for the full altitude range. Thus, relative values of NO_y species are well reproduced but not their absolute values. The NO/NO_2 ratio is correctly modelled by Reprobus 1-D for all the altitude range, except for altitudes lower

than 19 km. Since during high latitude summer the partitioning between NO and NO_2 is mainly governed by Reactions (R1) and (R2) the NO/NO_2 ratio can be approximated by:

$$\frac{[NO]}{[NO_2]} \approx \frac{J_{NO_2}}{k_1[O_3]} \quad (1)$$

Accordingly if the ozone concentration is overestimated, this ratio becomes smaller and the NO and NO_2 concentrations calculated with a photochemical steady state model are both underestimated. Measured vertical profiles of ozone by LPMA and DOAS experiments are compared to the calculated one on Fig. 5. Ozone volume mixing ratios are overestimated by the model for all the altitude range, in particular below 19 km where the relative difference between modelled and observed ozone is increasing. This overestimation could explain the underestimation of NO/NO_2 values for altitudes lower than 19 km (Fig. 4).

The model initialisation is very important in order to simulate the NO_y burden, thus a better initialisation, in particular for ozone and total NO_y amounts, is necessary. One way to initialise NO_y in the model would be to use the N_2O profile measured by LPMA and the observed correlation between N_2O and NO_y in the stratosphere. However, LPMA measurements of N_2O are not sufficiently accurate for a firm inter-comparison. Therefore in a second model run, we chose, to constrain the model initialisation by the LPMA measurements of total NO_y and ozone. For NO_y, the three dominant species (NO, NO_2 and HNO_3) are inferred from LPMA retrievals, and they represent between 90 and 95% of total NO_y depending on the considered altitude. The other NO_y species (N_2O_5, $ClONO_2$,...) are derived from the output of the 3-D simulation. The time (hh mm UT), the latitude λ and the longitude μ corresponding to each sounded tangent altitude during sunset and sunrise are reported in Tables 1 and 2. The simplified notation (λ, μ) *hh mm* is used in the following. No measurement was performed exactly at initialisation time, hh_i mm_i UT, (16:00 UT for sunset and 1:00 UT for sunrise) in the different locations (λ, μ). Then, the O_3 and NO_y profiles retrieved from LPMA during sunset

ACPD
4, 8171–8199, 2004

and sunrise have to be scaled to their estimated value at 16:00 UT and 1:00 UT. This value is computed from the actual measurements, scaled by the variation predicted by the model between the initialisation time and the measurement time. We apply Eq. (2) to the volume mixing ratio of species X for each relevant tangent altitude reported in Tables 1 and 2, i.e. for each corresponding time ($hh\ mm$ UT) and location (λ, μ).

$$X_{LPMA}^{(\lambda,\mu)hh_i\,mm_i} = \frac{X_{Reprobus}^{(\lambda,\mu)hh_i\,mm_i}}{X_{Reprobus}^{(\lambda,\mu)hh\,mm}} X_{LPMA}^{(\lambda,\mu)hh\,mm} \quad (2)$$

Note that constraining the model with LPMA measurements somewhat disturbs the balance within the NO_y family, as minor NO_y species are not measured. Thus, before analysing the results, the 1-D model is run for about 4 to 50 days (depending of the considered altitude) until a satisfactory balance is reached.

Using this model initialisation, a very good agreement between measured and modelled vertical profiles of NO, NO_2 and HNO_3 is observed at sunset and sunrise (cf. Fig. 6). Except for a slight overestimation of NO between 20 and 24 km, the volume mixing ratio values of NO, NO_2 and HNO_3 are well reproduced by the model. A reasonably good agreement is also obtained for $ClONO_2$, as shown on Fig. 7. The measured NO_x/NO_y profile is then well reproduced by the model, as for the first model initialisation with the CTM Reprobus (Fig. 8a). The percentage difference between measured NO_x/NO_y profiles and corresponding calculated values for sunset and sunrise is lower than 5% for altitudes higher than 30 km and of the order of 15% for altitudes lower than 30 km and the difference never exceeds 25%. The model reproduces very well the partitioning between NO and NO_2. In particular, this second model run shows a better agreement with LPMA below 19 km, as a result of the more realistic ozone initialisation in this altitude range (Fig. 8b). Between 25 and 40 km the NO/NO_2 percentage difference is smaller than 10% and 5% for sunset and sunrise, respectively. For altitudes lower than 25 km, this difference changes more with the observed conditions and it is of the order of 30% at sunrise. For sunset the discrepancy is around 20% for the three lowest altitudes, whereas the simulated ratios do not fall within the range given

ACPD
4, 8171–8199, 2004

by the error bars at 22 km. We believe that this discrepancy can be explained best by an incomplete coincidence of measurement and model times since the instruments assigns two consecutive spectra to the same line of sight and in consequence to the same tangent altitude. These two spectra correspond to a forward (when the moving mirror of the Michelson interferometer moves away from zero path difference or ZPD, Zero Path Difference) and a reverse (fly back of the mirror to ZPD) interferograms. The duration of this round-trip is around 100 s. A given LOS (Line Of Sight) and time are assigned to a reverse and forward scan sharing almost the same ZPD in the middle of this 100 s interval. The tangent altitude varies of several hundred meters and of the order of 0.1° in latitude and longitude during the recording time. Times and locations indicated in Table 1 and 2 are consequently mean times and locations and this is true for the tangent altitude of two consecutive spectra. The uncertainty on the time and location of the tangent point could explain a part of the discrepancy observed between calculated and measured values of NO/NO_2.

We further test the influence of the aerosol burden on simulated NO_y. The previous results were obtained with the aerosol burden usually chosen in the Reprobus CTM seasonal calculations. This aerosol distribution is not completely realistic, however, in particular for altitudes lower than 20 km. In another model sensitivity test, we thus use the aerosol surface area profile (below 30 km) deduced from balloon-borne aerosol measurements performed in 2002 (Deshler, 2003). It is important to note that the accuracy of the measured aerosol surface area is only 40% and that the variability of aerosol surface area values between two consecutive years is quite large for altitudes lower than 18 km. The aerosol surface area profile measured from Deshler in 2002 is available down to 10 km (the last tangent altitude probed by LPMA at sunset is around 13 km). The comparison of calculated and measured NO_x/NO_y profiles is presented on Fig. 9. The partitioning of NO_x and NO_y is governed by both gas-phase and heterogeneous chemistry. Although heterogeneous reactions involving N_2O_5 are not important in the polar summer stratosphere, the impact of aerosol burden initialisation is not negligible for NO, NO_2 and HNO_3 (from 10% to 25% on average, not shown). Taking into ac-

count a more realistic measured stratospheric aerosol burden is largely improving the agreement between calculated and measured NO_x/NO_y profiles (cf. Fig. 9). This is especially true below 20 km, where CTM strongly underestimates aerosol. With the new surface area profile, model-observation percentage differences are then smaller than 10% over the covered altitude range, except for the lowest altitude, where it reaches 13%. Very similar results are observed for the sunrise comparison (not shown).

4. Conclusions

The LPMA/DOAS balloon-borne solar occultation measurements performed over Kiruna (Sweden) on 21–22 August 2001 allowed us to check our understanding of the NO_y and NO_x partitioning during polar summer. In order to test the measured versus simulated NO_y partitioning, we used a state-of-art chemical transport model that includes the most recent gas-phase rate coefficients, absorption cross-sections and heterogeneous reactions as recommended by the NASA JPL2003 compilations. Vertical profiles of NO, NO_2, HNO_3, NO/NO_2 and NO_x/NO_y, deduced from LPMA measurements are compared to the corresponding profiles calculated with the Reprobus 1-D model. Different model initialisations are tested and we show that measurements and calculations are in good agreement (both absolute concentrations and mixing ratios) when the photochemical model is constrained by measured ozone and total NO_y. This confirms earlier results obtained by Osterman et al. (1999) and Gao et al. (1999) that using the 2003 updated JPL reaction rate coefficients for the partitioning of NO_y, much of the earlier disagreement between measured and modelled stratospheric NO_x and NO_y disappears for the polar summer stratosphere. Moreover, taking realistic stratospheric aerosol burdens, cf. from the Deshler 2002 measurements, leads to a significantly better agreement.

References

Bösch, H., Camy-Peyret, C., Chipperfield, M., Fitzenberger, R., Harder, H., Schiller, C., Schneider, M., Trautmann, T., and Pfeilsticker, K.: Inter comparison of measured and modeled stratospheric UV/vis actinic fluxes at large solar zenith angles, Geophys. Res. Lett., 28, 1179–1182, 2001.

Brown, S. S., Talukdar, R. K., and Ravishankara, A. R.: Rate constants for the reaction OH + NO_2 + M → HNO_3 + M under atmospheric conditions, Chem. Phys. Lett., 229, 277–284, 1999a.

Brown S. S., Talukdar, R. K., and Ravishankara, A. R.: Reconsideration of the rate constant for the reaction of hydroxyl radicals with nitric acid, J. Phys. Chem. A, 103, 3031–3037, 1999b.

Camy-Peyret, C., Jeseck, P., Hawat, T., Durry, G., Payan, S., Berubé, G., Rochette, L., and Huguenin, D.: The LPMA balloon-borne FTIR spectrometer for remote sensing of atmospheric constituents, ESA Publications SP-370, 323–328, 1995.

DeMore, W. B., Sander, S. P., Golden, D. M., et al.: Chemical kinetics and photochemical data for use in stratosphere odeling, JPL Publ. 97-4, Jet Propul. Lab., Pasadena, Calif., 1997.

Deshler, T., Hervig, M. E., Hofmann, D. J., Rosen, J. M., and Liley, J. B.: Thirty years of in situ stratospheric aerosol size distribution measurements from Laramie, Wyoming (41° N), using balloon-borne instruments, J. Geophys. Res., 108, 4167–4179, 2003.

Ferlemann, F., Bauer, N., Fizenberger, R., Harder, H., Osterkamp, H., Perner, D., Platt, U., Scheider, M., Vradelis, P., and Pfeilsticker, K.: A new DOAS-instrument for stratospheric balloon-borne trace gas studies, Appl. Opt., 39, 2377–2386, 2000.

Gao, R. S., Fahey, D. W., Del Negro, L. A., Donnelly, S. G., Keim, E. R., Neuma, J. A., Teverovskaia, E., Wennberg, P. O., Hanisco, T. F., Lanzendorf, E. J., Proffitt, M. H., Margitan, J. J., Wilson, J. C., Elkins, J. W., Stimpfle, R. M., Cohen, R. C., McElroy, C. T., Bui, T. P., Salawitch, R. J., Brown, S. S., Ravishankara, A. R., Portmann, R. W., Ko, M. K. W., Weisenstein, D. K., and Newman, P. A.: A comparison of observations and model simulations of NO_x/NO_y in the lower stratosphere, Geophys. Res. Lett., 26, 1153–1156, 1999.

Lary, D. J., Toumi, R., Lee, A. M., Newchurch, M., Pirre, M., and Renard, J.-B.: Carbon aerosols and atmospheric photo-chemistry, J. Geophys. Res., 102, 3671–3682, 1997.

Lefèvre, F., Brasseur, G., Folkins, I., Smith, A. K., and Simon, P.: Chemistry of the 1991–1992 stratospheric winter: Three dimensional model simulations, J. Geophys. Res., 99, 8183–8195, 1994.

Lefèvre, F., Figarol, F., Carslaw, K. S., and Peter, T.: The 1997 Arctic ozone depletion quantified from three-dimensional model simulations, Geophys. Res. Lett., 25, 2425–2428, 1998.

Osterman, G. B., Sen, B., Toon, G. C., Salawitch, R. J., Margitan, J. J., and Blavier, J. F.: Partitioning of NO_y species in the summer Arctic stratosphere, Geophys. Res. Lett., 26, 1157–1160, 1999.

Payan, S., Camy-Peyret, C., Jeseck, P., Hawat, T., Pirre, M., Renard, J. B., Robert, C., Lefèvre, F., Kanzawa, H., and Sasano, Y.: Diurnal and nocturnal distribution of stratospheric NO_2 from solar and stellar occultation measurements in the Arctic vortex: Comparison with models and ILAS satellite measurements, J. Geophys. Res., 104, 21 585–21 593, 1999.

Perkins, K. K., Hanisco, T. F., Cohen, R. C., Koch, L. C., Stimpfle, R. M., Voss, P. B., Bonne, G. P., Lanzendorf, E. J., Anderson, J. G., Wennberg, P. O., Gao, R. S., Del Negro, L. A., Salawitch, R. J., McElroy, C. T., Hintsa, E. J., Loewenstein, M., and Bui, T. P.: The NO_x-HNO_3 system in the lower stratosphere: Insights from in situ measurements and implications of the J_{HNO3}-[OH) relationship, J. Phys. Chem. A, 105, 1521–1534, 2001.

Rothman, L. S., Rinsland, C. P., Goldman, A., et al.: The HITRAN molecular database: edition of 2000 including updates through 2001, JQSRT, 82, 5–44, 2003.

Sander, S. P., Friedl, R. R., Golden, D. M., et al.: Chemical kinetics and photochemical data for Use in atmospheric studies, NASA/JPL Evaluation, JPL Publication 02-25, 2002. Only online: http://jpldataeval.jpl.nasa.gov.

Sen, B., Toon, G. C., Osterman, G. B., Blavier, J.-F., Margitan, J. J., Salawitch, R. J., and Yue, G. K.: Measurements of reactive nitrogen in the stratosphere, J. Geophys. Res., 103, 3571–3585, 1998.

Thomason, L. W., Poole, L. R., and Deshler, T. R.: A Global Climatology Of Stratospheric Aerosol Surface Area Density As Deduced From SAGE II: 1984–1994, J. Geophys. Res., 102, 8967–8976, 1997.

Wagner, G. and Birk, A.: New infrared spectroscopic database for chlorine nitrate, JQSRT, 82, 443–460, 2003.

Wennberg, P. O., Cohen, R. C., Stimpfle, R. M., Koplow, J. P., Anderson, J. G., Salawitch, R. J., Fahey, D. W., Woodbridge, E. L., Keim, E. R., Gao, R. S., Webster, C. R., May, R. D., Toohey, D. W., Avallone, L. M., Proffitt, M. H., Loewenstein, M., Podolske, J. R., Chan, K. R., and Wofsy, S. C.: Removal of stratospheric O_3 by radicals: In situ measurements of OH, HO_2, NO_2, ClO and BrO, Science, 266, 398–404, 1994.

Wetzel, G., Oelhaf, H., von Clarmann, T., Fischer, H., Friedl-Vallon, F., Maucher, G., Seefeldner,

M., and Trieschmann, O.: Vertical profiles of N_2O_5, HO_2NO_2 and NO_2 inside the Arctic vortex retrieved from nocturnal MIPAS-B2 infrared limb emission measurements in February 1995, J. Geophys. Res., 102, 19 177–19 186, 1997.

Table 1. Time, latitude and longitude of LPMA sunset measurements for selected tangent altitudes H_t.

Time (UT)	Latitude	Longitude	H_t (km)
18:45	68.07	21.01	38.68
18:50	68.32	20.21	38.29
18:55	68.59	19.44	37.69
19:00	68.86	18.71	36.77
19:05	69.14	18.01	35.51
19:10	69.43	17.34	33.96
19:15	69.73	16.71	32.25
19:20	70.03	16.12	30.34
19:25	70.33	15.57	28.10
19:30	70.61	15.13	26.11
19:35	70.91	14.70	23.79
19:40	71.20	14.38	21.60
19:45	71.48	14.11	19.30
19:50	71.75	13.91	17.16
19:55	72.04	13.70	14.75
19:59	72.26	13.58	13.06

ACPD
4, 8171–8199, 2004

Table 2. Time, latitude and longitude of LPMA sunrise measurements for selected tangent altitudes H_t.

Time (UT)	Latitude	Longitude	H_t (km)
1:18	71.31	31.91	16.31
1:25	70.98	31.55	19.02
1:30	70.70	31.13	21.56
1:35	70.43	30.68	23.94
1:40	70.16	30.19	26.10
1:45	69.86	29.61	28.44
1:50	69.56	28.99	30.60
1:55	69.27	28.33	32.60
2:00	68.99	27.63	34.35
2:05	68.71	26.90	35.84
2:10	68.45	26.14	37.05
2:15	68.19	25.34	38.04
2:20	67.94	24.51	38.67
2:25	67.70	23.66	39.02

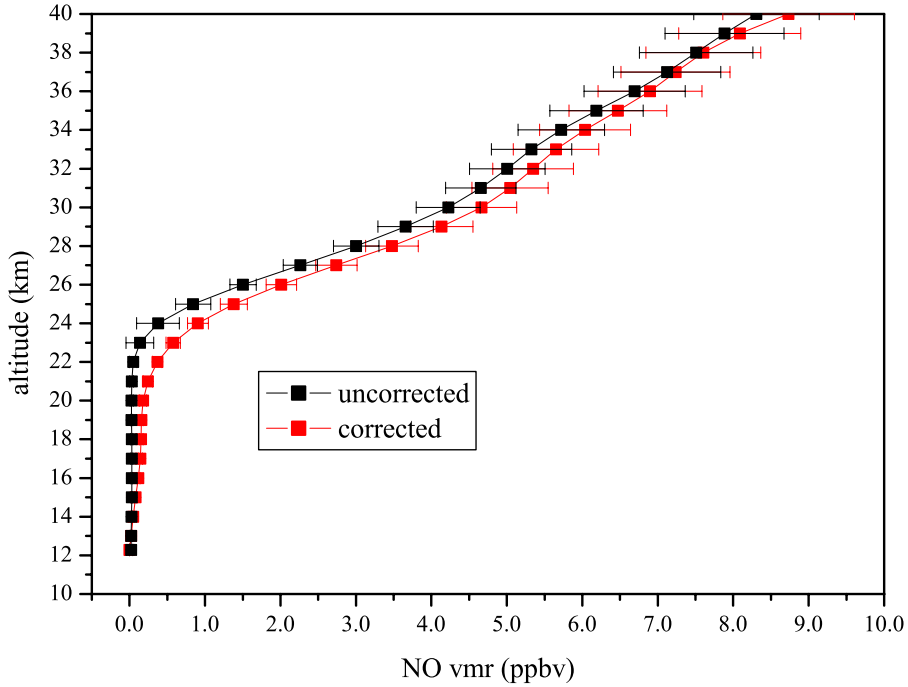

Fig. 1. Comparison between NO vertical profiles retrieved with or without accounting for the photochemical variations along the line of sight.

ACPD
4, 8171–8199, 2004

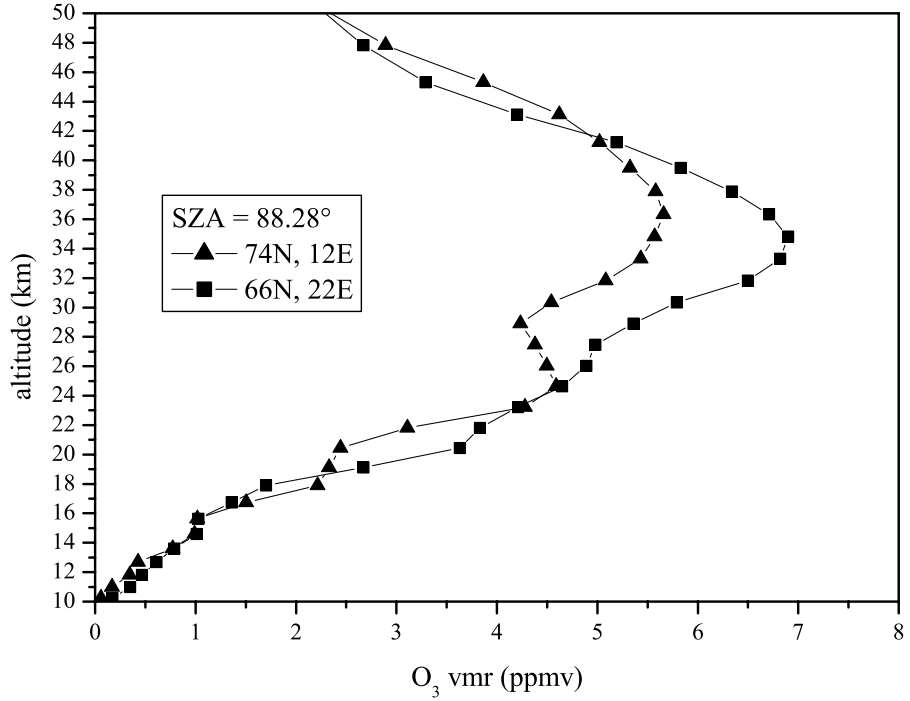

Fig. 2. Sensitivity to location (latitude, longitude) of O_3 and NO_2 mixing ratio profiles during sunset. Vertical profiles are inferred from the three-dimensional photochemical model, Reprobus. They are calculated at the same solar zenith angle (88.28°) and at the two model grid points (74° N, 12° E) and (66° N, 22° E) nearest to the two extreme sunset locations of the tangent point measured.

ACPD
4, 8171–8199, 2004

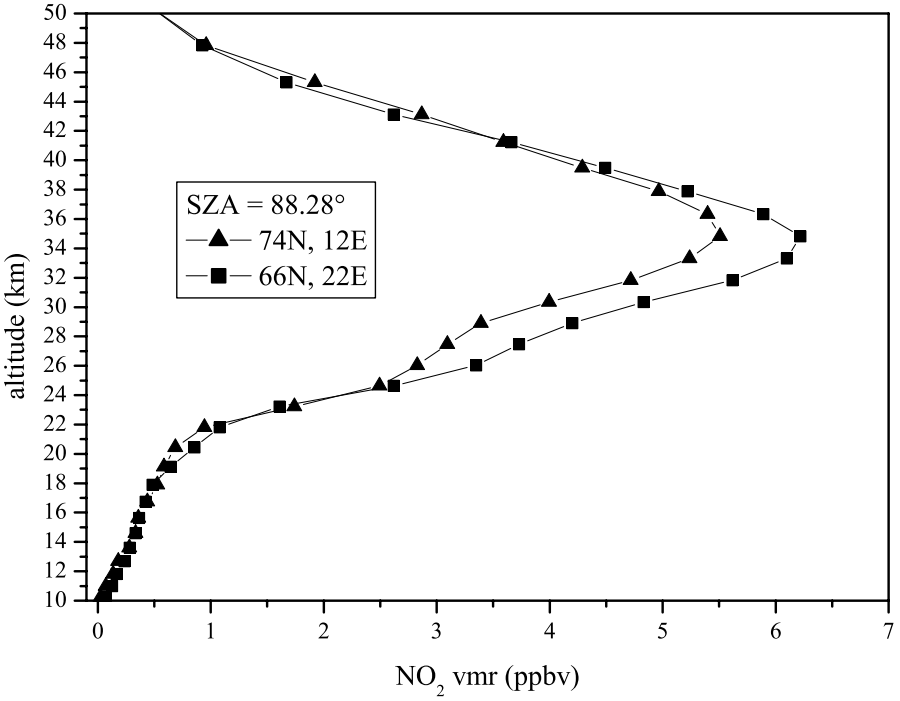

Fig. 2. Continued.

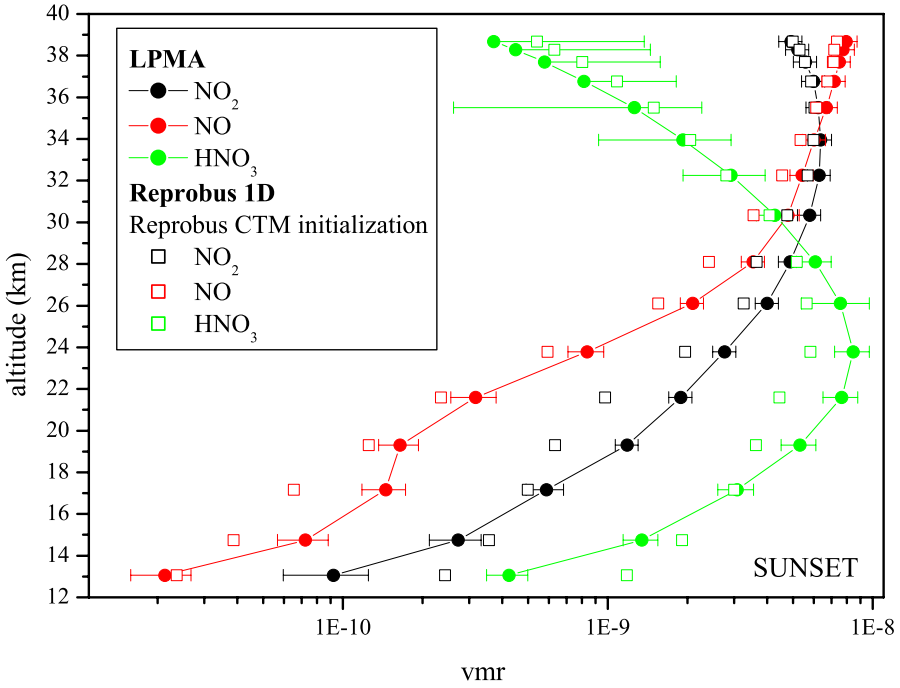

Fig. 3. Comparison between measured NO, NO_2 and HNO_3 profiles during sunset and corresponding calculated profiles with the Reprobus 1-D model initialised with Reprobus CTM.

ACPD
4, 8171–8199, 2004

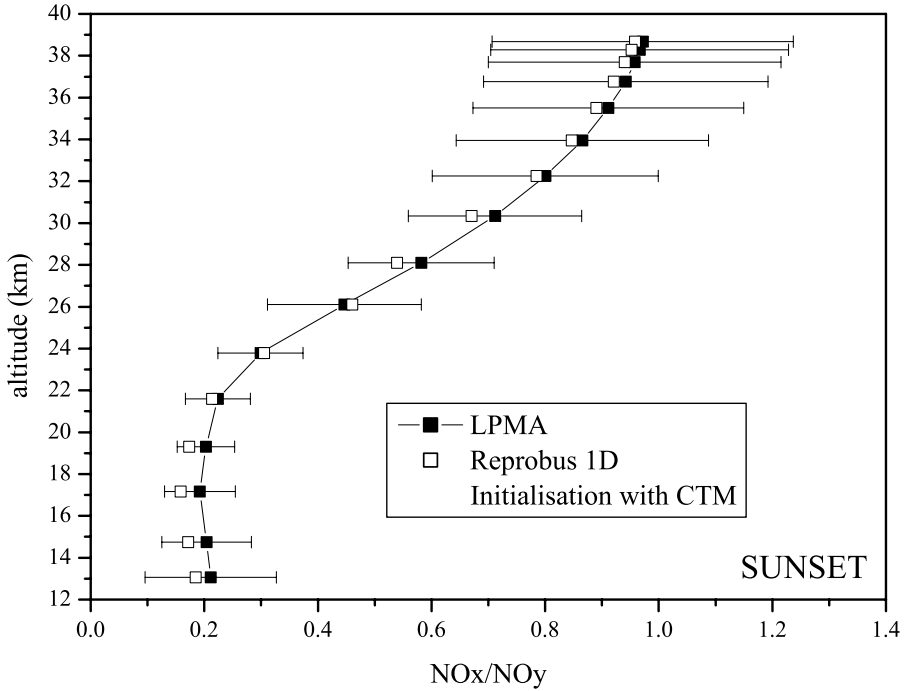

Fig. 4. (a) Comparison between measured NO_x/NO_y profile during sunset and the corresponding calculated profile with the Reprobus 1-D model initialised with Reprobus CTM.

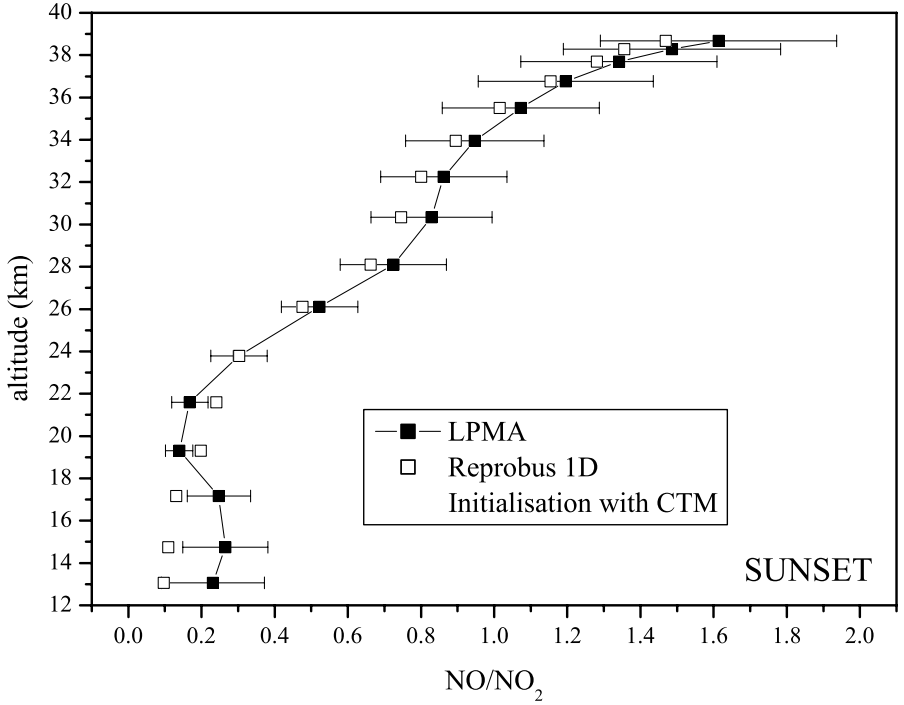

Fig. 4. (b) Comparison between measured NO/NO_2 profile during sunset and the corresponding calculated profile with the Reprobus 1-D model initialised with Reprobus CTM.

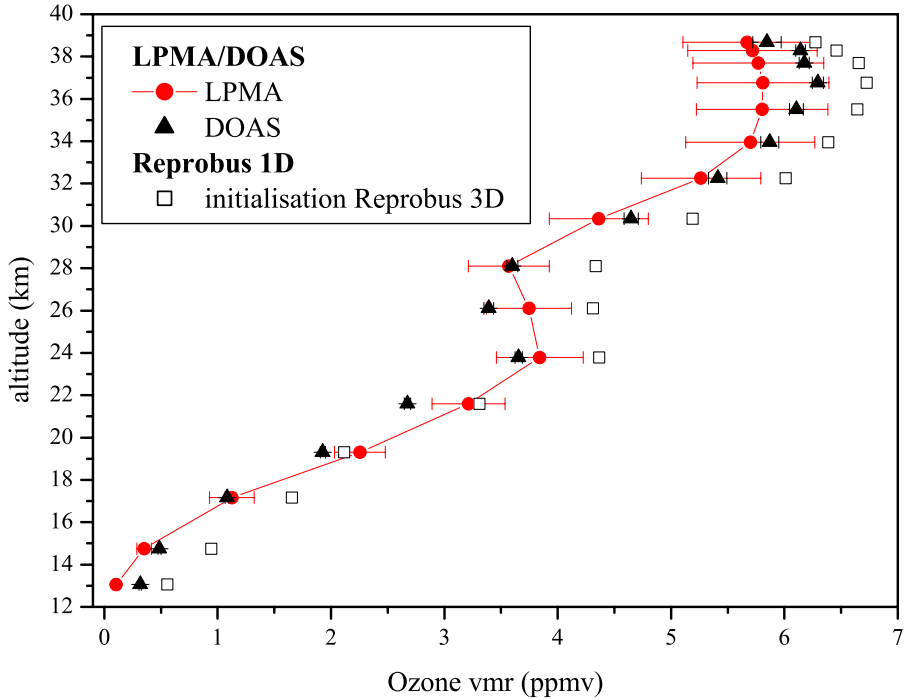

Fig. 5. Ozone vertical profile measured by LPMA and by DOAS (below 19 km) is compared to profiles measured by DOAS and calculated by the Reprobus 1-D model initialised with Reprobus CTM.

ACPD
4, 8171–8199, 2004

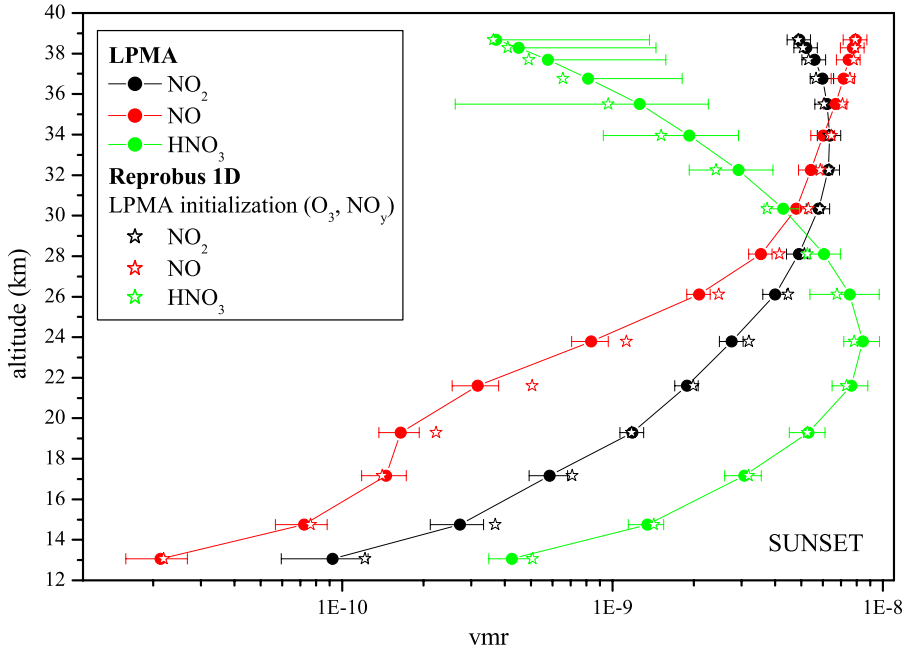

Fig. 6. **(a)** Comparison between measured NO, NO_2 and HNO_3 profiles during sunset and corresponding calculated profiles with the Reprobus 1-D model constrained by measured O_3 and NO_y amounts.

ACPD
4, 8171–8199, 2004

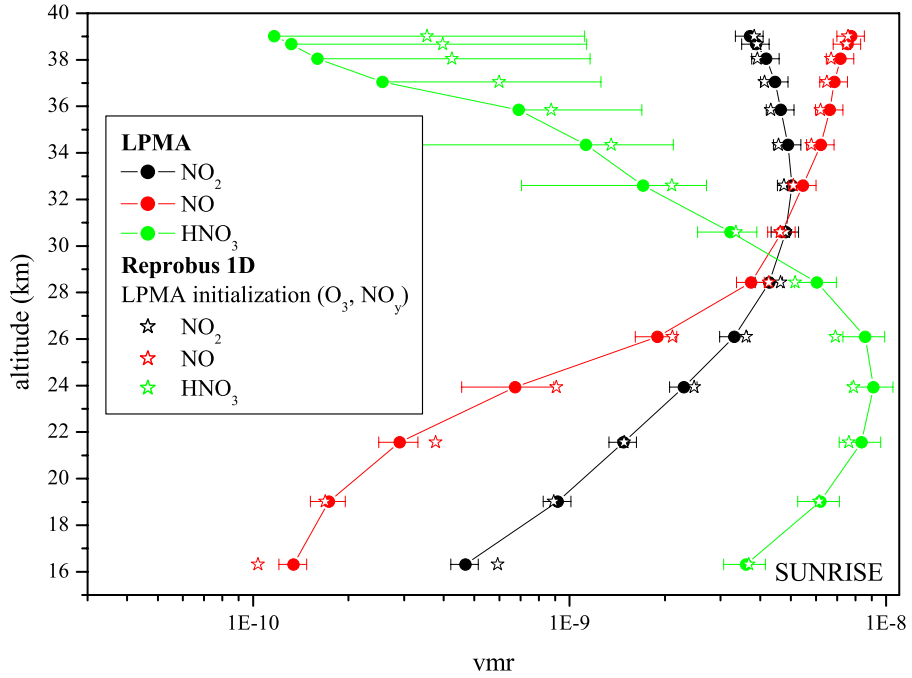

Fig. 6. (b) Comparison between measured NO, NO_2 and HNO_3 profiles during sunrise and corresponding calculated profiles with the Reprobus 1-D model constrained by measured O_3 and NO_y amounts.

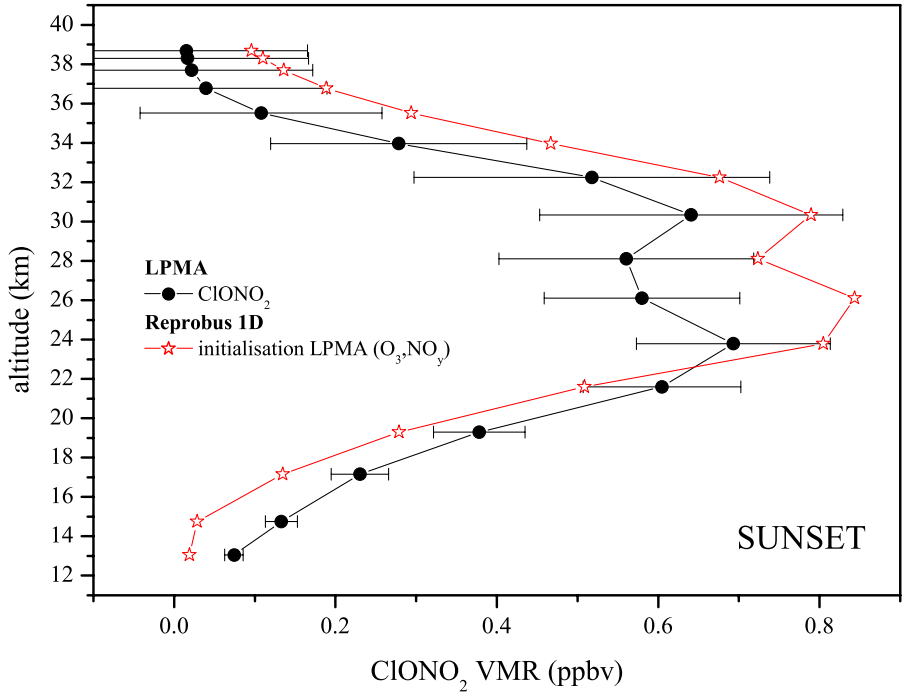

Fig. 7. Comparison between measured $ClONO_2$ profile during sunset and corresponding calculated profiles with the Reprobus 1-D model constrained by measured O_3 and NO_y amounts.

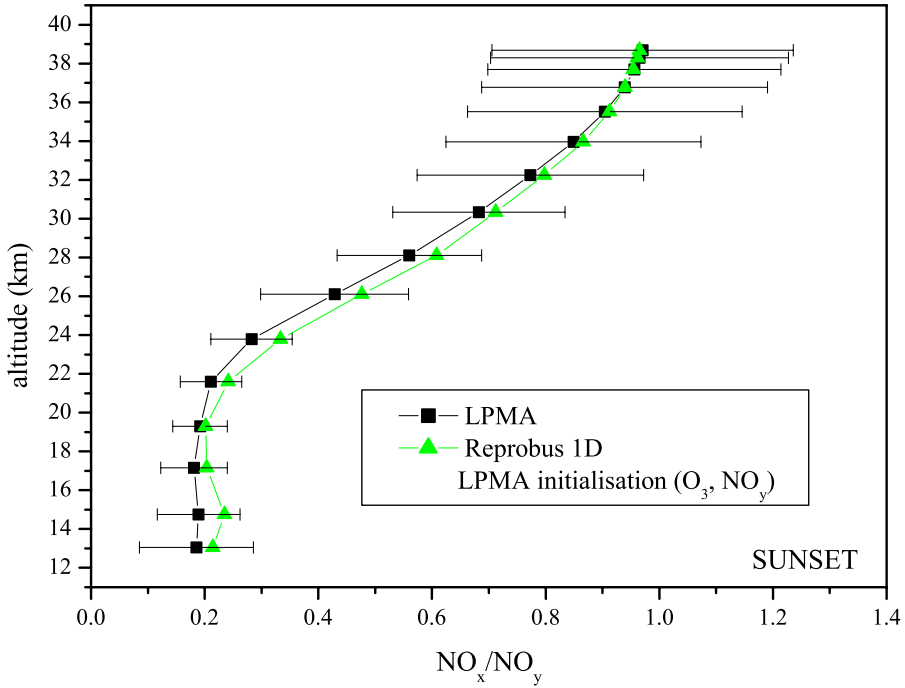

Fig. 8. **(a)** Comparison between measured NO_x/NO_y profiles during sunset and the corresponding calculated profile with the Reprobus 1-D model constrained by measured O_3 and NO_y amounts.

ACPD
4, 8171–8199, 2004

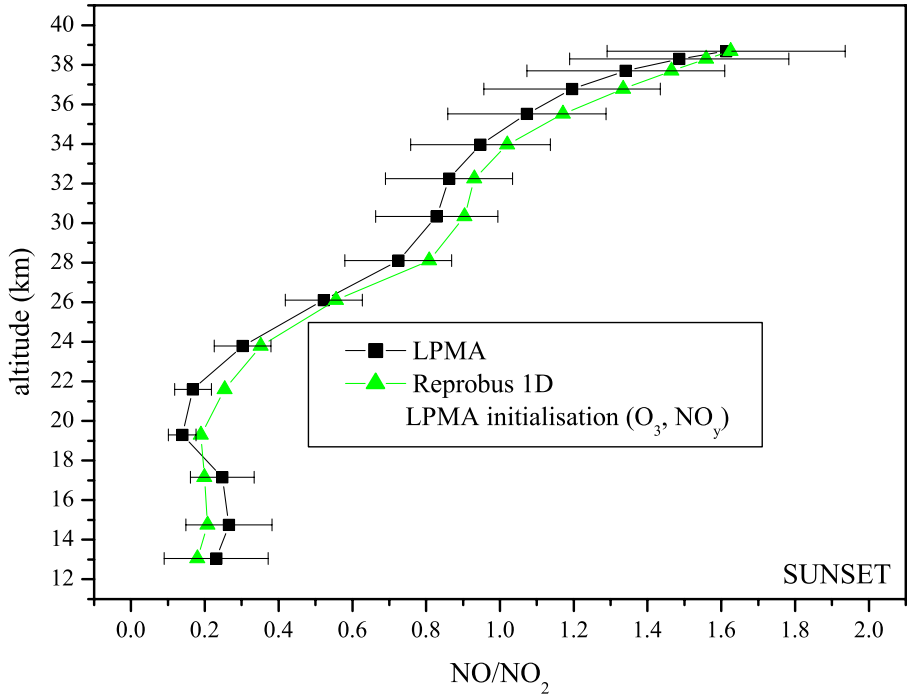

Fig. 8. **(b)** Comparison between measured NO/NO_2 profiles during sunset and the corresponding calculated profile with the Reprobus 1-D model constrained by measured O_3 and NO_y amounts.

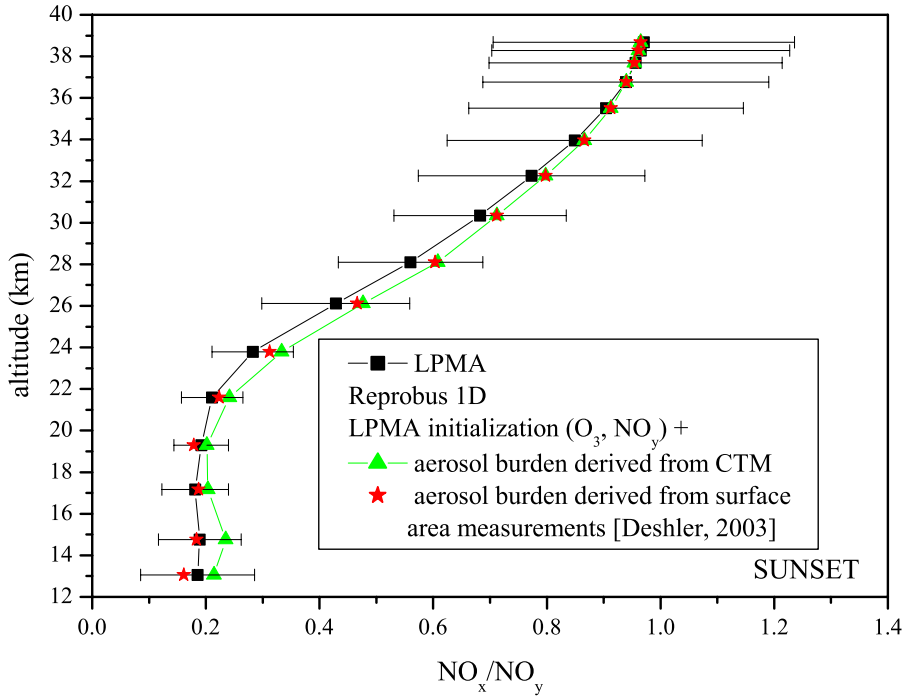

Fig. 9. Comparison between measured NO_x/NO_y profiles during sunset and the corresponding calculated profile with the Reprobus 1-D model constrained by measured O_3 and NO_y amounts and initialised with aerosol burden derived from CTM calculations or from surface area measurements.